Mixed-isotope Bose-Einstein condensates in rubidium

Valery S. Shchesnovich,[1,*] Anatoly M. Kamchatnov,[1,2,†] and Roberto A. Kraenkel[1,‡]
[1]*Instituto de Física Teórica, Universidade Estadual Paulista-UNESP, Rua Pamplona 145, 01405-900 São Paulo, Brazil*
[2]*Institute of Spectroscopy, Russian Academy of Sciences, Troitsk 142190, Moscow Region, Russia*
(Received 8 August 2003; revised manuscript received 13 October 2003; published 3 March 2004)

We consider the ground-state properties of mixed Bose-Einstein condensates of ^{87}Rb and ^{85}Rb atoms in the isotropic pancake trap for both signs of the interspecies scattering length. In the case of the repulsive interspecies interaction, there are the axially symmetric and symmetry-breaking ground states. The threshold for the symmetry-breaking transition, which is related to appearance of a zero dipole mode, is found numerically. For attractive interspecies interactions, the two condensates assume symmetric ground states for the numbers of atoms up to the collapse instability of the mixture.

DOI: 10.1103/PhysRevA.69.033601 PACS number(s): 03.75.Mn, 03.75.Hh

I. INTRODUCTION

Bose-Einstein condensation (BEC) in mixtures of trapped quantum gases has become an exciting field of study. The first experimental observation of the two-species BEC was realized using two different spin states of ^{87}Rb [1]. The two overlapping condensates of ^{87}Rb in the spin states $|F=1,m=-1\rangle$ and $|F=2,m=2\rangle$ were created via nearly lossless sympathetic cooling of the atoms in the state $|2,2\rangle$ by thermal contact with the atoms in the $|1,-1\rangle$ state. Also, the double-condensate system of ^{87}Rb in the spin states $|1,-1\rangle$ and $|2,1\rangle$ was created from the single condensate in the $|1,-1\rangle$ state by driving a two-photon transition [2]. In the subsequent evolution after creation, the condensates underwent complex relative motions, preserving the total density profile. The motions quickly damped out and the condensates assumed a steady state with a non-negligible (and adjustable) overlap region. These experiments started a series of works devoted to experimental and theoretical studies of BEC in mixtures. For instance, superposition of the spinor condensates of ^{23}Na led to the observation of weakly miscible and immiscible superfluids [3] and the occurrence of metastable states [4]. An interaction between two condensates of different spin states of ^{87}Rb in the displaced traps was observed in center-of-mass oscillations [5]. Successful attempts to cool fermion gases to the quantum degeneracy regime by using boson-fermion mixtures were also reported. The first such mixture was achieved by using the two species of Li, the bosonic ^{7}Li and fermionic ^{6}Li [6,7]. More recently, experiments on mixtures of different atomic species were performed. Both boson-boson and boson-fermion pairs were cooled. The two species BEC of ^{41}K and ^{87}Rb [8] and boson-fermion mixtures ^{87}Rb$-^{40}$K [9,10] and ^{23}Na–^{6}Li [11] were achieved.

A promising combination for obtaining the two-species BEC potentially rich in new phenomena is the mixture of two isotopes of rubidium: ^{85}Rb and ^{87}Rb. There is a long-standing interest in obtaining this BEC mixture, which goes back to Ref. [12], where the feasibility of achieving such two-species BEC was established. It was suggested that condensation of the two isotopes of rubidium can be achieved via the sympathetic cooling of certain hyperfine states which exhibit low inelastic collision rates. Moreover, the possibility of employing the Feshbach resonance for control over the scattering length was stressed. The optimal combination was found to be the mixture of the spin states $|2,-2\rangle_{85}$ and $|1,-1\rangle_{87}$, because the scattering length *between* the isotopes can be controlled. Sympathetic cooling of the ^{85}Rb condensate by thermal contact with the ^{87}Rb condensate was subsequently experimentally demonstrated [13]. Up to 10^6 atoms of the ^{85}Rb isotope were cooled via elastic collisions with a large reservoir (10^9 atoms) of ^{87}Rb. The stable condensate of the ^{85}Rb isotope was also created by using the Feshbach resonance to reverse the sign of the scattering length from negative to positive [14]. In this way, long-living condensates with up to 10^4 atoms of ^{85}Rb in the spin state $|2,-2\rangle$ were produced.

One of the principal advantages of using the rubidium isotopes is that their interspecies and intraspecies scattering lengths are known with a good precision [12]; thus theoretical predictions can be compared with the experiment. In particular, the scattering lengths of the ^{87}Rb isotope and between the two isotopes are positive, while the scattering length of the ^{85}Rb isotope is negative.

Efficient interspecies thermalization crucially depends on the interspecies scattering length and the overlap region of the species. It is known that spatial separation may take place depending on the values of the scattering lengths. If all atomic interactions in the mixture are repulsive, the following simple criterion for the spatial separation of two BECs in a box [15] is known: if the mutual repulsion is large enough—namely, $G_{12}>\sqrt{G_{11}G_{22}}$ (where G_{ij} is the interaction coefficient)—the condensates separate to lower the energy. The symmetry-breaking point of view on the ground state in the mixture of condensates was developed in Refs. [16–20]. For instance, by taking an equal number of atoms in the two species, the symmetry-preserving versus symmetry-breaking phase diagram was obtained in Ref. [18]. The existence of metastable states in the BEC mixtures was argued also on the basis of the Bogoliubov excitation spectra in Ref.

*Electronic address: valery@ift.unesp.br
†Electronic address: kamch@isan.troitsk.ru
‡Electronic address: kraenkel@ift.unesp.br

[21], where both signs of the interspecies scattering length were considered (for repulsive intraspecies interactions). In Ref. [22] two-species condensates with coinciding positive or negative interspecies scattering lengths and equal numbers of atoms in the species were considered within a variational approach. However, the results of the latter work do not apply to the BEC mixture of the two isotopes of rubidium, where, first of all, the interspecies scattering lengths have different signs. Finally, the collapse of a two-component BEC in the spherically symmetric trap was numerically studied in Ref. [23], where all possible combinations of the signs of the atomic interactions for the two species were considered. It was found that, depending on the interaction coefficients, either one or both components may experience collapse.

In related theoretical studies of boson-fermion mixtures [24–29] all possible signs of the boson and boson-fermion *s*-wave scattering lengths were considered (due to the strong *s*-wave scattering between bosons and fermions, the *p*-wave contribution to the interspecies interaction is neglected; see Refs. [26,29]). This reflects the fact that in experiments on boson-fermion mixtures various combinations of signs are possible; for instance, the two-isotope mixture of lithium of Ref. [6] had attractive boson and repulsive boson-fermion interactions, while in Ref. [7] the same species were used in different angular momentum states with repulsive atomic interactions. Though the governing equations for the boson-fermion mixture are different from those for the two-boson BEC, the predicted effects, such as the phase separation [24,27,29] and collapse [28,29], have similar features. In Ref. [29] a comprehensive analysis of the properties of boson-fermion mixtures for all possible signs of the boson and boson-fermion *s*-wave scattering lengths is given. We will make connections to the results of the latter work in the following sections.

In the present paper we study two-species BEC in a pancake trap for the numbers of atoms below the collapse instability. Our main goal is to understand the ground state of the two-species BEC mixture comprised of ^{85}Rb and ^{87}Rb isotopes, with the atoms being in the optimal spin states $|2,-2\rangle_{85}$ and $|1,-1\rangle_{87}$. We consider both attractive and repulsive interspecies interactions for fixed (default) intraspecies interactions with scattering lengths −412.5 a.u. (−21.8 nm) for $|2,-2\rangle_{85}$ and 107.5 a.u. (5.7 nm) for $|1,-1\rangle_{87}$—the averages of those given in Ref. [12]. In Sec. II we introduce the two-dimensional model describing the two-species BEC mixture in a pancake trap (i.e., the trap with a strong confinement in one direction) and discuss the domain of its applicability. Then, we present the numerically found ground states in the BEC mixture of the two isotopes of rubidium for the repulsive as well as attractive interspecies interactions, Secs. III A and III B, respectively. The concluding Sec. IV contains a brief summary of the results. The detailed derivation of the two-dimensional model is placed in Appendix A, while details of the stability analysis of the axially symmetric ground states are given in Appendix B.

II. TWO-DIMENSIONAL MODEL FOR THE PANCAKE TRAP

We consider a two-species BEC mixture in the isotropic pancake trap for arbitrary intraspecies and interspecies scattering lengths. The Gross-Pitaevskii equations for the two-species BEC have the form [30]

$$i\hbar\partial_t\Psi_1 = -\frac{\hbar^2}{2m_1}\nabla^2\Psi_1 + V_1(\boldsymbol{r})\Psi_1 + (G_{11}|\Psi_1|^2 + G_{12}|\Psi_2|^2)\Psi_1, \tag{1a}$$

$$i\hbar\partial_t\Psi_2 = -\frac{\hbar^2}{2m_2}\nabla^2\Psi_2 + V_2(\boldsymbol{r})\Psi_2 + (G_{22}|\Psi_2|^2 + G_{12}|\Psi_1|^2)\Psi_2, \tag{1b}$$

where $\Psi_1(\boldsymbol{r},t)$ and $\Psi_2(\boldsymbol{r},t)$ are the order parameters of the two species, while the interaction coefficients are given as $G_{11}=4\pi\hbar^2 a_1/m_1$, $G_{22}=4\pi\hbar^2 a_2/m_2$, and $G_{12}=2\pi\hbar^2 a_{12}/M$, with a_1, a_2, and a_{12} being the intraspecies and interspecies scattering lengths, respectively. Here M denotes the reduced mass: $M=m_1m_2/(m_1+m_2)$. In our case, for the two isotopes of rubidium, we can neglect the mass difference between the isotopes and take $m=m_1=m_2$. We consider the parabolic pancake trap

$$V_j = \frac{m\omega_{j,z}^2}{2}z^2 + \frac{m\omega_{j,\perp}^2}{2}r_\perp^2, \quad j=1,2, \tag{2}$$

with strong confinement in the z direction: $\gamma\equiv\omega_z/\omega_\perp \gg 1$ [by a simple phase transformation the possible difference of the zero-point energies for the two species in the trap can be scaled away from system (1)]. The difference in the magnetic trap frequencies felt by the two species is caused by the difference of the Lande magnetic factors for the two isotopes [30]: $g(|2,-2\rangle_{85})=-1/6$ and $g(|1,-1\rangle_{87})=-1/4$. The corresponding magnetic moments measured in the Bohr magnetons are given as follows: $\mu_{85}=g(|2,-2\rangle_{85})m_{85}=1/3$ and $\mu_{85}=g(|1,-1\rangle_{87})m_{87}=1/4$. Hence, the ratio of the squared trap frequencies is $\omega_{87}^2/\omega_{85}^2=\mu_{87}/\mu_{85}=3/4$, where ω_{85} and ω_{87} stand for the frequencies experienced by the respective isotopes. From now on, the indices 1 and 2 will correspond to the isotopes ^{85}Rb and ^{87}Rb, respectively.

For not too large numbers of atoms the three-dimensional system (1) can be reduced to a system of two-dimensional equations in the pancake coordinates $\boldsymbol{r}_\perp=(x,y)$, while the order parameter in the z direction is fixed and given by the Gaussian. Indeed, the motion in the z direction is quantized under the condition that the energy contribution from the nonlinearity be much less than the difference between the energy levels of the trap:

$$\frac{|G_{j1}|N_1}{d_{1,z}d_{1,\perp}^2} \ll \hbar\omega_{1,z}, \quad \frac{|G_{j2}|N_2}{d_{2,z}d_{2,\perp}^2} \ll \hbar\omega_{2,z}, \quad j=1,2. \tag{3}$$

Here we have estimated the order parameter as $|\Psi_j|^2 \sim N_j/(d_{j,z}d_{j,\perp}^2)$, $j=1,2$, with the introduction of the effective sizes of the condensates in the pancake plane ($d_{j,\perp}$) and in the z direction ($d_{j,z}$). Under condition (3), the z sizes of the condensates are given by the trap size: $d_{j,z}=a_{j,z}$, with $a_{j,z}$ being the respective oscillator length in the z direction [see formula (4)], whereas their sizes in the pancake plane must be determined from the solution to the resulting two-dimensional system [system (6) below]. We will reformulate

condition (3) in a more convenient form below. More detailed analysis of the two-dimensional (2D) approximation is placed in Appendix A.

Under condition (3) the order parameter Ψ_j is approximated as a product of the Gaussian wave function in the z direction and a wave function describing the transverse shape:

$$\Psi_j = e^{-i\omega_{j,z}t/2} f_j(z)\Phi_j(\boldsymbol{r}_\perp, t),$$

$$f_j \equiv \pi^{-1/4} a_{j,z}^{-1/2} \exp\left(-\frac{z^2}{2a_{j,z}^2}\right), \quad a_{j,z} \equiv \left(\frac{\hbar}{m\omega_{j,z}}\right)^{1/2}. \quad (4)$$

The Gaussian is the ground-state wave function of the linear part of the right-hand side (RHS) in system (1) which corresponds to quantum motion in the z direction: $H_{j,z} \equiv -\hbar^2/(2m)\partial_z^2 + m\omega_{j,z}^2 z^2/2$, with $H_{j,z} f_j(z) = (\hbar\omega_{j,z}/2) f_j(z)$. Substitution of expression (4) in system (1), multiplication of the equation for Ψ_j by $f_j(z)$ and integration over z results in the approximate two-dimensional system [see also Eqs. (A3) and (A4) in Appendix A]. To write it down in a form convenient for numerical calculations, let us introduce the dimensionless variables

$$\boldsymbol{\rho} = \frac{\boldsymbol{r}_\perp}{a_\perp}, \quad a_\perp \equiv \left(\frac{\hbar}{m\omega_\perp}\right)^{1/2}, \quad T = \frac{\omega_\perp}{2} t, \quad \psi_j = a_\perp \Phi_j,$$

$$j = 1, 2. \quad (5)$$

Here we have defined the frequency $\omega_\perp$ as $\omega_\perp^2 = (\omega_{1,\perp}^2 + \omega_{2,\perp}^2)/2$, where $\omega_{j,\perp}$, $j=1,2$, are the trap frequencies in the pancake plane experienced by the two isotopes. Then the dimensionless approximate 2D system reads

$$i\partial_T \psi_1 = -\nabla_\perp^2 \psi_1 + \lambda_1^2 \rho^2 \psi_1 + (g_{11}|\psi_1|^2 + g_{12}|\psi_2|^2)\psi_1, \quad (6a)$$

$$i\partial_T \psi_2 = -\nabla_\perp^2 \psi_2 + \lambda_2^2 \rho^2 \psi_2 + (g_{22}|\psi_2|^2 + g_{12}|\psi_1|^2)\psi_2, \quad (6b)$$

where $\rho = |\boldsymbol{\rho}|$,

$$g_{11} = \frac{4\sqrt{2\pi}a_1}{a_{1,z}}, \quad g_{22} = \frac{4\sqrt{2\pi}a_2}{a_{2,z}}, \quad g_{12} = \frac{8\sqrt{\pi}a_{12}}{(a_{1,z}^2 + a_{2,z}^2)^{1/2}},$$

$$\lambda_1 = \frac{\omega_{1,\perp}}{\omega_\perp}, \quad \lambda_2 = \frac{\omega_{2,\perp}}{\omega_\perp}. \quad (7)$$

Using the relation $\omega_2^2/\omega_1^2 = 3/4$ for the rubidium isotopes in the spin states $|2,-2\rangle_{85}$ and $|1,-1\rangle_{87}$, we obtain $\lambda_1^2 = 8/7$ and $\lambda_2^2 = 6/7$.

The pancake trap sizes in the experiments on BEC have different values. To set a reference for discussion, in the calculations below we assume the z size of the trap to be 10 μm; i.e., we set $a_{1,z} = 10$ μm ($a_{2,z} = 2.03^{-1/4} a_{1,z} = 0.84 a_{1,z}$). This results in the following values for the interaction coefficients in the mixture of the two isotopes of rubidium: $g_{11} = -0.0219$, $g_{22} = 0.0068$, and $g_{12} = 0.012$. For a different trap size the interaction coefficients will change. However, the quantities $g_{11}N_1$, $g_{22}N_2$, $g_{12}N_2$, and $g_{12}N_1$, computed from a solution to system (6), will remain invariant under variation of the trap size. Thus, a different trap size a_z will result in a similar solution but for an appropriately scaled numbers of atoms. We will return to this point below.

Let us now reformulate condition (3) in a form more convenient for verification. Scaling the sizes of the condensates in the pancake plane by the respective trap length, $d_{j,\perp} = R_j a_\perp$, we obtain the equivalent conditions in the form of the bounds on the numbers of atoms:

$$N_1 \ll \gamma \frac{R_1^2}{4\pi} \min\left(\frac{a_z}{|a_1|}, \frac{a_z}{|a_{12}|}\right), \quad N_2 \ll \gamma \frac{R_2^2}{4\pi} \min\left(\frac{a_z}{|a_2|}, \frac{a_z}{|a_{12}|}\right), \quad (8)$$

where a_z denotes both $a_{1,z}$ and $a_{2,z}$, since they have close values, and $\gamma \gg 1$ ($\gamma = \omega_z/\omega_\perp = a_\perp^2/a_z^2$). The sizes R_1 and R_2 of the two condensates must be determined from the solution of system (6). For instance, for the pancake trap with $a_z = 10$ μm, using the values of the scattering lengths from Sec. I for the ^{85}Rb-^{87}Rb mixture, we obtain the following bounds: $N_j \ll 10^2 \gamma R_j^2$, $j=1,2$. The actual bounds on the numbers of atoms are thus determined by the trap anisotropy γ. For example, if $\gamma = 100$ (i.e., $a_\perp = 10 a_z$), we have $N_j \ll 10^4 R_j^2$.

There is the critical number of atoms, N_c, such that the ^{85}Rb condensate, in the absence of the other isotope, is unstable with respect to collapse for $N_{85} > N_c$. By setting $g_{12} = 0$ in the two-dimensional system (6), we obtain the following expression for the critical number of ^{85}Rb atoms necessary for collapse (in the absence of the other isotope):

$$N_c = \frac{2\pi I_0}{|g_{11}|} = \frac{\sqrt{\pi} I_0}{2\sqrt{2}} \frac{a_{1,z}}{|a_1|} = \kappa_{2D} \frac{a_{1,z}}{|a_1|}, \quad (9)$$

where $\kappa_{2D} = 1.167$. In the derivation of formula (9) we have used the well-known condition for collapse in the critical nonlinear Schrödinger equation (for details consult Ref. [31]) and that the number of particles, N_0, in the so-called Townes soliton is $N_0 = 2\pi I_0$, where $I_0 = 1.862$.

It is important to notice that both the upper bound (8) on the admissible numbers of atoms and the threshold number for collapse (9) in the ^{85}Rb condensate are proportional to the trap size in the z direction. Thus, taking a bigger pancake trap (with the same γ) will relax the bounds on the numbers of atoms. The threshold for collapse in the mixture of the two isotopes of rubidium also depends on the number of atoms of the ^{87}Rb isotope. However, we have found numerically that this dependence is very weak (the correction does not exceed 5 % for the numbers of atoms used below and the fixed default scattering lengths); therefore, the threshold given by Eq. (9) can be taken as a good approximation. For example, for the pancake trap with $a_z = 10$ μm, used above, the threshold for collapse is $N_c = 535$.

Finally, let us comment on the validity of the approximate 2D system for a description of the collapse instability in the mixture. First of all, one may point out that the threshold value for collapse of the mixture in the pancake trap determined from the full three-dimensional system (1) may turn out to be lower than that predicted by the two-dimensional

approximation, as is true, for instance, for the single-species condensate of ^{85}Rb. Indeed, in the latter case, the exact (i.e., 3D) threshold can be written as $N_c=\kappa(\gamma)a_z/|a_1|$ [32]. Using the numerically found values of $\kappa(\gamma)$ from Ref. [32], we conclude that $\kappa(\gamma)<\kappa_{2D}$ for any $\gamma>1$; i.e., this inequality holds for any pancake trap. As $\gamma\to\infty$, the function $\kappa(\gamma)$ slowly tends to κ_{2D}. For example, for the trap with $a_z=10$ μm and $\gamma=100$ we have $\kappa(100)=1.1$ [32], which gives 95 % (506 atoms) of the threshold given by formula (9).

Nevertheless, in the pancake trap, the instability which is solely due to the three-dimensionality is weak if the conditions given by Eq. (8) are satisfied and the numbers of atoms are not much greater than the corresponding instability threshold. This conclusion follows from the general discussion of the 2D approximation, which is placed in Appendix A. Here we note also that the instability rate due to the 3D effects decreases with increase of the trap anisotropy γ [since it enters the RHS's of the conditions in Eq. (8)]. Therefore, in a sufficiently anisotropic pancake trap, the 3D collapse instability below the threshold of the 2D collapse does not have enough time to develop on the time scale set by the two-dimensional system (6) and, hence, its effect on the solutions can be neglected. In fact, the time necessary for such a weak instability to develop may exceed the lifetime of the condensates in the mixture.

It is, however, the *dynamics* of a collapsing condensate in the pancake trap that cannot be treated in the framework of the two-dimensional approximation and requires the full 3D analysis due to violation of at least one of the two conditions (8). Thus we will not discuss such dynamics. For more details on the two-species collapse in BEC's consult, for instance, Ref. [23] and on the collapse in boson-fermion mixtures consult Refs. [28,29].

In the case of the two-species BEC of ^{85}Rb and ^{87}Rb, there is a stable state in the mixture, predicted by the 2D system (6) for numbers of atoms slightly lower than the collapse instability (see the next section), which violates the applicability conditions (8) for modest pancake traps ($\gamma\leqslant 100$) due to sharp contraction of the ^{85}Rb condensate. The sharp decrease of the ^{85}Rb condensate size R_1, predicted by system (6), requires a large trap anisotropy γ for the 2D system to sustain its validity. Therefore, for the current experimental traps, the very existence of such exotic states requires a full 3D analysis and thus is beyond the 2D approximation adopted in the present paper. We will not discuss such states either.

Therefore, for the current experimental pancake traps, the applicability of the approximate 2D system (6) is limited by the threshold of formation of the contracted states in the ^{85}Rb condensate. In the next section we discuss the ground states in the mixture for the allowed numbers of atoms and their deformations due to the instabilities predicted by the 2D system, such as the symmetry-breaking transition. Such instabilities are much stronger than those due to three-dimensional effects and, consequently, are observed on a much shorter time scale (consult also Appendix A).

III. GROUND STATES IN THE MIXTURE OF TWO ISOTOPES OF RUBIDIUM

Now we turn to the numerical solution of system (6) to find possible ground states in the BEC mixture of the two isotopes. Stationary solutions are sought for in the usual form

$$\psi_1 = e^{-i\mu_1 T}U_1(\rho), \quad \psi_2 = e^{-i\mu_2 T}U_2(\rho), \tag{10}$$

where μ_1 and μ_2 are dimensionless chemical potentials for the two species. We have used the gradient method for the constrained energy minimization to find $U_1(\rho)$ and $U_2(\rho)$ minimizing the energy functional,

$$\mathcal{E} = \int \mathrm{d}^2\boldsymbol{\rho}\Big\{ |\nabla_\perp \psi_1|^2 + |\nabla_\perp \psi_2|^2 + \rho^2(\lambda_1^2|\psi_1|^2 + \lambda_2^2|\psi_2|^2) + \frac{g_{11}}{2}|\psi_1|^4 + \frac{g_{22}}{2}|\psi_2|^4 + g_{12}|\psi_1\psi_2|^2\Big\}, \tag{11}$$

for fixed numbers of atoms $N_1=\int \mathrm{d}^2\boldsymbol{\rho}|\psi_1|^2$ and $N_2=\int \mathrm{d}^2\boldsymbol{\rho}|\psi_2|^2$.

A. Ground states for repulsive interspecies interaction

Let us start with considering the BEC mixture of ^{85}Rb and ^{87}Rb atoms with the repulsive interspecies interaction. First of all, we have found the axially symmetric ground states via the energy minimization restricted to the space of the axially symmetric functions. It is important to know if the symmetric states are stable. The stability analysis can be based on the method of Refs. [33,34], whose adaptation to our problem is described in Appendix B. We have found that the axially symmetric ground state of the mixture suffers from the dipole-mode symmetry-breaking instability for a sufficiently large number of atoms in the ^{87}Rb condensate and not too large numbers of atoms in the ^{85}Rb condensate ($N_{85}\leqslant 500$). The symmetry breaking instability was previously discussed for the case of BEC mixtures in Refs. [16–20]. The novelty here lies in the fact that one of the condensates has an attractive atomic interaction. For instance, the separation criterion of Ref. [15] for a BEC mixture in the box—i.e., $g_{12}>\sqrt{g_{11}g_{22}}$—loses its meaning since in our case $g_{11}g_{22}<0$ and, *a priori*, it is not evident that the isotopes would separate at all.

The axially symmetric ground states on the threshold of the symmetry-breaking instability for various numbers of atoms are shown in Fig. 1. It should be stressed that there are three types of *stable* axially symmetric states in the system for smaller numbers of atoms, which correspond (and are similar) to the threshold states shown in Fig. 1: (i) when the isotopes are strongly mixed (the two condensates have bell-shaped form, the dotted lines), (ii) when the ^{85}Rb isotope is on the surface of ^{87}Rb ($|\psi_1|$ has a local minimum at the center, the solid lines), and (iii) when the ^{87}Rb isotope is on the surface of ^{85}Rb isotope ($|\psi_2|$ has a local minimum at the center, the dashed lines).

The threshold of the symmetry-breaking instability strongly depends on the numbers of atoms and corresponds to appearance of a zero dipole mode (which pertains to the orbital operator Λ_{11}; consult Appendix B). From the energetic point of view, the separation takes place when the energy gain due to the intraspecies interaction in the strongly mixed state is higher than the kinetic energy (quantum pres-

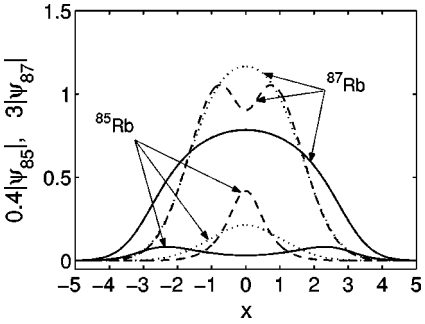

FIG. 1. The three types of the axially symmetric state in the mixture of ^{85}Rb and ^{87}Rb isotopes on the threshold of the symmetry-breaking instability. The one-particle wave functions are shown (scaled for better visibility as is indicated on the *y* axis). The numbers of atoms are as follows. Solid lines: $N_{85}=100$ and $N_{87}=17412$. Dotted lines: $N_{85}=300$ and $N_{87}=2042$. Dashed lines: $N_{85}=450$ and $N_{87}=894$.

sure) at the interface between the separated condensates. The corresponding symmetry-breaking diagram, found numerically, is given in Fig. 2.

Though all three types of axially symmetric ground states discussed above suffer from the symmetry-breaking instability with increase of the number of atoms of the ^{85}Rb isotope (for sufficiently large number of atoms of the ^{87}Rb isotope), the symmetry-restored states (found to the right of the phase separation curve in Fig. 2), which result from a further increase of the number of ^{85}Rb atoms, are of type (iii)—i.e., when the ^{87}Rb isotope is on the surface of the ^{85}Rb isotope.

In the reduced 2D system (6), with a further increase of the number of ^{85}Rb atoms the symmetry-restored state of type (iii) is immediately followed by a sharp contraction of the ^{85}Rb condensate and the subsequent collapse at $N_{85}\approx 535$. The collapse instability is due to appearance of the axially symmetric unstable mode (i.e., the unstable linear mode with orbital number $l=0$; see Appendix B). The collapse threshold value of N_{85} only slightly decreases with an increase of the number of ^{87}Rb atoms. This is due to the very favorable set of default scattering lengths of the system and

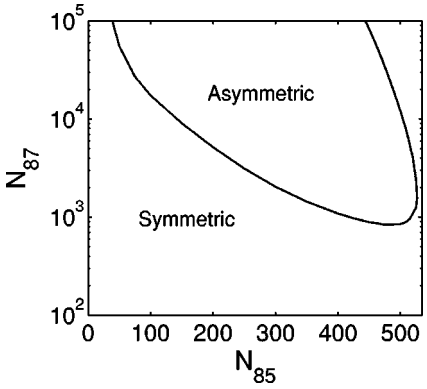

FIG. 2. The symmetric vs asymmetric ground-state diagram. The interaction coefficients are $g_{11}=-0.0219$, $g_{22}=0.0068$, and $g_{12}=0.012$ (computed for default values of the scattering lengths and $a_{1,z}=10\ \mu$m). The logarithmic (base 10) scale is used for the ^{87}Rb axis.

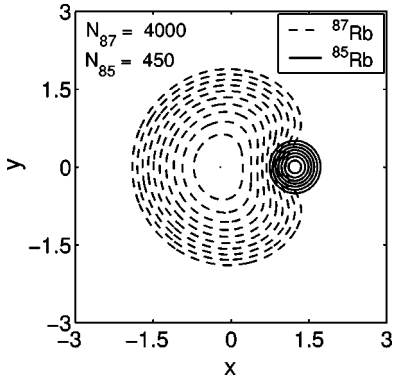

FIG. 3. The symmetry-breaking ground state for a not too large number of ^{87}Rb atoms. For each of the two condensates, the equidistant level curves ranging from the maximum of the order parameter to a half of its value are shown.

is not a general property of the mutually repulsive mixtures of attractive and repulsive species. For instance, in a related study of the boson-fermion mixtures, it was noted that though the collapse in the mutually repulsive boson-fermion mixture with attractive boson interactions only concerns the boson species, it can be strongly affected by the fermion number of atoms [29]. However, for such an effect to be pronounced, the interspecies *s*-wave scattering length must be significantly larger than the absolute value of the boson scattering length.

Thus, right before the collapse instability the size of the ^{85}Rb condensate first decreases to a fraction of the trap size $a_\perp$. However, depending on the trap anisotropy γ, such a state may violate the first of the two applicability conditions (8) for the 2D approximation. For example, our estimates show that an accurate description of this effect requires a full 3D analysis for pancake traps with $\gamma\leqslant 100$. For observations of this effect, much more anisotropic pancake traps are required, which are not used in the current experiments. Thus we will not discuss the effect any further. There is also an implication of the validity of a part of Fig. 2 for the current pancake traps: the 2D approximation for the pancake trap with $\gamma\leqslant 100$ is not valid for a description of the symmetric ground states to the right of the separation curve except for a narrow strip immediately after it (with the width equal to a dozen of atoms on the N_{85} axis).

The symmetry-breaking ground states are illustrated in Figs. 3 and 4, where we show the contour lines of the order parameters (ranging from the maximum to half of its value at a constant step) for ^{85}Rb (solid lines) and ^{87}Rb (dashed lines). We have found that it is the ^{85}Rb condensate that is expelled from the center of the trap in the symmetry-breaking states. It is seen that for comparable numbers of atoms of the two species it is the ^{87}Rb condensate that suffers the strongest deformation from the bell-shaped form, while for $N_{87}\gg N_{85}$ the ^{85}Rb condensate is strongly deformed. Here we note that the asymmetric ground state of the mixture is degenerate, as it possesses the rotational zero mode. In other words, the maximum of the order parameter of ^{85}Rb can have an arbitrary position angle on the surface of the ^{87}Rb condensate.

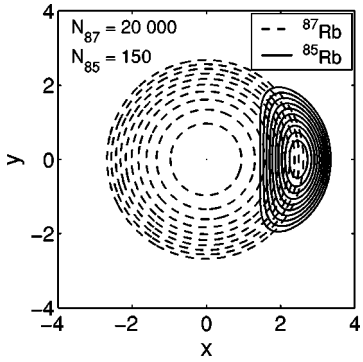

FIG. 4. The asymmetric ground state for a very large number of ^{87}Rb atoms. The equidistant level curves are shown with the range defined as in the previous figure.

B. Ground states for attractive interspecies interaction

Now let us consider the BEC mixture of two isotopes when the interspecies interaction is attractive, which can be experimentally realized by using the Feshbach resonance [12]. It is convenient to measure the interspecies interaction coefficient g_{12} in terms of the interaction coefficient g_{11} of the ^{85}Rb isotope. We have found that the condensates do not separate in this case and assume the axially symmetric ground state up to the collapse instability threshold. Such ground states are illustrated in Fig. 5, where we plot the appropriately scaled one-particle wave functions for the two condensates. Note the local peak at the center of the ^{87}Rb condensate. The appearance of this peak is easy to understand, for instance, when the Thomas-Fermi limit applies to the ^{87}Rb condensate (which corresponds to the picture in the lower panel of Fig. 5). Indeed, if $N_{87} \gg N_{85}$, then in the zero-order approximation one can neglect the contribution from the interspecies interaction term $g_{12}|\psi_1|^2$ in Eq. (6) for the ^{87}Rb condensate in the region away from the trap center. Thus, in the zero-order approximation, the ^{87}Rb condensate

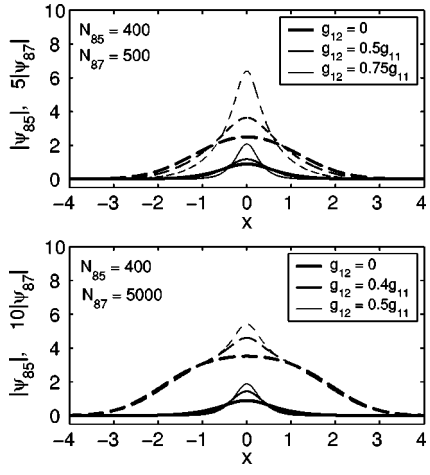

FIG. 5. Stable ground states of the BEC mixture for the attractive interspecies interactions. The one-particle wave functions (scaled for better visibility as indicated along the *y* axis) are shown. In both panels, the solid lines correspond to the ^{85}Rb isotope and the dashed lines to the ^{87}Rb isotope.

has the Thomas-Fermi ground state independently of the state of the other isotope. Therefore the effect of the cross-interaction term $g_{12}|\psi_2|^2$ in the equation for the ^{85}Rb condensate, Eq. (6), is now similar to that of an additional potential. In the next order of approximation, the order parameter ψ_2 of the ^{87}Rb condensate is a sum of the two terms: the background Thomas-Fermi shape and the local deformation at the center of the trap. The latter is determined by the order parameter of the ^{85}Rb condensate. It is interesting to note that a similar central density enhancement of the fermion species in boson-fermion mixtures with attractive interspecies interactions is predicted in Ref. [29] (Figs. 1 and 2).

It should be noted that, notwithstanding the attraction in the ^{85}Rb condensate and the attractive interspecies interaction, the ground states shown in Fig. 5 are not self-bound; i.e., they are not solitons: relaxation of the trap results in spreading of the condensates.

Finally, lowering of the interspecies interaction coefficient g_{12} to sufficiently large negative values results in a sharp contraction of the ^{85}Rb condensate which is followed by collapse instability. This contraction of the *stable* ground state of the ^{85}Rb condensate to a fraction of the trap size is due to the presence of the other condensate, since the size of a stable single species BEC is always on the order of the trap size.

Thus, as in the case of the repulsive interspecies interactions, the collapse instability in the mixture is preceded by a sharp decrease of the ^{85}Rb condensate size. Therefore, depending on the trap anisotropy γ, its description may take us beyond the 2D approximation adopted in this paper. For most of the current pancake traps $\gamma \leqslant 100$; thus, the description of the ground state in the mixture which is on the border of the collapse instability requires a full three-dimensional analysis.

We note, however, that for small values of $|g_{12}|$ the stable symmetric ground states predicted by the 2D approximation and illustrated in Fig. 5 can be experimentally observed in the current pancake traps with $\gamma \sim 100$. In such an experiment, the number of ^{85}Rb atoms should be below the threshold value $N_c = N_c(N_{87})$ which, for fixed g_{12}, decreases only by a few percent from the value given by formula (9) with an increase of the number of ^{87}Rb atoms.

IV. CONCLUSION

We have studied the ground state in the BEC mixture of two isotopes of rubidium in the pancake trap for repulsive and attractive interspecies interactions and fixed (default) intraspecies interactions.

In the case of repulsion between the two species, there is the symmetry-breaking deformation of the ground state due to the dipole-mode instability, whose threshold strongly depends on the numbers of atoms of the two isotopes. For small numbers of atoms—i.e., below the symmetry-breaking instability threshold—the stable axially symmetric ground state has the form of either the strongly mixed state of the species (with the order parameters of the two condensates having bell-shaped form) or the state where one of the condensates forms a circular strip on the surface of the other.

For attractive interspecies interactions, the condensates assume axially symmetric ground states for all numbers of atoms where the 2D approximation is valid. For small values of the (negative) interspecies interaction coefficient $|g_{12}|$ the mixture is stable for the numbers of ^{85}Rb atoms below the critical value $N_c = N_c(N_{87})$ which is a few percent lower than the collapse instability threshold for a single-species condensate of ^{85}Rb (i.e., for $g_{12}=0$). There is a sharp peak in the density of the repulsive ^{87}Rb isotope due to the attractive interspecies interactions—the effect which is similar to the enhancement of the fermionic density in boson-fermion mixtures with attractive boson-fermion interactions [29].

Finally, for pancake traps with anisotropy $\gamma \leqslant 100$, the 2D approximation for the attractive as well as repulsive mixture is violated at the numbers of atoms in the ^{85}Rb condensate just below the collapse instability in the 2D model due to the sharp contraction of the ^{85}Rb condensate. This is quite dissimilar to the case of the single-species BEC of ^{85}Rb, where the collapse sets in at a state which has a size comparable to the trap size in the pancake plane. Thus, investigation of the actual ground state of the mixture in such pancake traps at the numbers of atoms close to the collapse instability requires a full three-dimensional analysis and is beyond the approach adopted in the present paper. This sets a direction for future research.

ACKNOWLEDGMENTS

This work was supported by the FAPESP of Brazil. A.M.K. would like to thank the Instituto de Física Teórica—UNESP for kind hospitality.

APPENDIX A: DERIVATION OF THE TWO-DIMENSIONAL APPROXIMATION

The system (1) can be rewritten in the form

$$i\hbar\partial_t\Psi_1 = (H_{1z} + H_{1\perp} + G_{11}|\Psi_1|^2 + G_{12}|\Psi_2|^2)\Psi_1, \quad \text{(A1)}$$

$$i\hbar\partial_t\Psi_2 = (H_{2z} + H_{2\perp} + G_{22}|\Psi_2|^2 + G_{12}|\Psi_1|^2)\Psi_2, \quad \text{(A2)}$$

where we have introduced linear operators corresponding to quantum motion along the z axis and on the (x,y) plane in the trap:

$$H_{jz} = -\frac{\hbar^2}{2m_j}\frac{\partial^2}{\partial z^2} + V_{jz}(z), \quad H_{j\perp} = -\frac{\hbar^2}{2m_j}\nabla_\perp^2 + V_{j\perp}(\boldsymbol{r}_\perp),$$

$$j = 1,2.$$

The solution to Eqs. (A1) and (A2) can be expanded over the eigenfunctions of the linear operators H_{1z} and H_{2z} as follows: $\Psi_j = \Psi_{j0}(z,\boldsymbol{r}_\perp,t) + \hat{\Psi}_j(z,\boldsymbol{r}_\perp,t)$, $j=1,2$, where $\Psi_{j0} \equiv e^{-iE_{j0}t/\hbar} f_j(z)\Phi_j(\boldsymbol{r}_\perp,t)$, with $f_j(z)$ being the normalized eigenfunction of the ground state, $H_{jz} f_j(z) = E_{j0} f_j(z)$, while the second term $\hat{\Psi}_j$ is the projection of order parameter Ψ_j on the subspace orthogonal to the ground state.

We can expand the system (A1) and (A2) in similar way using the projectors Π_1 and Π_2 on the ground states of H_{1z} and H_{2z}, respectively. Application of these projectors to Eqs. (A1) and (A2) leads to a system describing the evolution of the projection of the order parameters for the two species on the respective ground states:

$$i\hbar\partial_t\Phi_1 = (H_{1\perp} + \tilde{G}_{11}|\Phi_1|^2 + \tilde{G}_{12}|\Phi_2|^2 + \Delta_1)\Phi_1 + \mathcal{F}_1, \quad \text{(A3)}$$

$$i\hbar\partial_t\Phi_2 = (H_{2\perp} + \tilde{G}_{22}|\Phi_2|^2 + \tilde{G}_{12}|\Phi_1|^2 + \Delta_2)\Phi_2 + \mathcal{F}_2, \quad \text{(A4)}$$

where $\tilde{G}_{ij} = G_{ij}\langle f_i^2 f_j^2\rangle$, with $\langle F\rangle \equiv \int F dz$,

$$\Delta_j = G_{jj}\langle f_j^2(2f_i\ \mathrm{Re}\{\Phi_j\hat{\Psi}_j^*\} + |\hat{\Psi}_j|^2)\rangle + G_{j,3-j}\langle f_j^2(2f_{3-j}\ \mathrm{Re}\{\Phi_{3-j}\hat{\Psi}_{3-j}^*\} + |\hat{\Psi}_{3-j}|^2)\rangle, \quad \text{(A5)}$$

and

$$\mathcal{F}_j = G_{jj}\langle f_j|\Psi_j|^2\hat{\Psi}_j\rangle + G_{j,3-j}\langle f_j|\Psi_{3-j}|^2\hat{\Psi}_j\rangle. \quad \text{(A6)}$$

On the other hand, the equations describing the evolution of the projections of the order parameters on the orthogonal subspaces are derived by application of the complementary projectors Q_j, $Q_j \equiv 1 - \Pi_j$ to the system (A1) and (A2):

$$i\hbar\partial_t\hat{\Psi}_1 = (\tilde{H}_{1z} + H_{1\perp})\hat{\Psi}_1 + Q_1\{G_{11}|\Psi_1|^2\Psi_1 + G_{12}|\Psi_2|^2\Psi_1\}, \quad \text{(A7)}$$

$$i\hbar\partial_t\hat{\Psi}_2 = (\tilde{H}_{2z} + H_{2\perp})\hat{\Psi}_2 + Q_2\{G_{22}|\Psi_2|^2\Psi_2 + G_{12}|\Psi_1|^2\Psi_2\}, \quad \text{(A8)}$$

where $\tilde{H}_{jz} = H_{jz} - E_{j0}$.

Let us estimate the orders of magnitude of the nonlinear terms in Eqs. (A3), (A4), (A7), and (A8) under the condition that the nonlinear terms in system (A1) and (A2) be much smaller than the characteristic difference $\Delta E \sim \hbar\omega_z$ between the eigenvalues of each of the two linear operators H_{1z} and H_{2z} [i.e., conditions (3) are satisfied]. Below we will not distinguish between quantities with different indices, since all quantities of the same kind are of the same order of magnitude. Introduce a small parameter ϵ as the ratio of the nonlinear terms in the system (A3) and (A4) to ΔE—that is,

$$\epsilon = \frac{\tilde{G}|\Phi|^2}{\Delta E} = \frac{G\langle f^4\rangle|\Phi|^2}{\Delta E}. \quad \text{(A9)}$$

Note that $\langle f^4\rangle \sim f^2$ since the integral of f^2 over z is of order 1. It is the smallness of ϵ, supposed in Eq. (3), that justifies the transition to the two-dimensional approximation. Indeed, the order of the correction $\hat{\Psi}$ to the factorized wave function can be found by equating the orders of the inhomogeneous term and the linear term $H_z + H_\perp$ in Eqs. (A7) and (A8), where, as in Eqs. (A3) and (A4), we have again $H_\perp\hat{\Psi} \sim \epsilon\Delta E\hat{\Psi}$ and $H_\perp$ can be neglected compared with $H_z \sim \Delta E$. Therefore, we get $\Delta E\hat{\Psi} \sim GQ\{|f\Phi|^2 f\Phi\} \sim \epsilon\Delta E f\Phi$ and, hence, $\hat{\Psi} \sim \epsilon f\Phi$. From this we obtain estimates for the terms given by Eqs. (A5) and

(A6): $\Delta \sim G\langle f^2 f\Phi\hat{\Psi}\rangle \sim \epsilon G f^2\Phi^2 \sim \epsilon^2\Delta E$ and $\mathcal{F} \sim G\langle f(f\Phi)^2\epsilon f\Phi\rangle \sim \epsilon G f^2\Phi^2\Phi \sim \epsilon^2\Phi\Delta E$.

Throwing away the terms of order ϵ^2 from Eqs. (A3) and (A4) and changing to the dimensionless variables given by Eq. (5) we arrive at the system (6). The projection of the order parameter Ψ_j on the orthogonal subspace, $\hat{\Psi}_j$, is of order ϵ and can be neglected compared to the factorized wave function $f_j\Phi_j$. We conclude that, under conditions (3), nonlinearity plays a significant role only on the pancake plane (x,y).

Two comments are in order on the two-dimensional approximation described above. First, the effects due to the three dimensionality of the mixture will be of order ϵ^2, the same order as the terms we have thrown out from the system (A3) and (A4); thus, they will give a significant contribution to the dynamics only on the time scale of order ϵ^{-2}, much longer than the time scale of the nonlinear effects in 2D, which is of order ϵ^{-1}. Second, a similar 2D approximation will be valid for the linearized system which describes the evolution of a small perturbation of the solution. Thus, any instability in the mixture which is solely due to its three dimensionality will be of order ϵ^2 and will not play any role in the time scale we consider.

The latter comment concerns, for instance, the instability due to collapse in 3D: although the 3D threshold value of the number of atoms in the mixture necessary for collapse may turn out to be lower than that in the 2D approximation, as is true for the single-species condensate of ^{85}Rb, the corresponding instability rate (proportional to the unstable eigenvalue) will be of order ϵ^2 and will not be noticed on the time scale we consider.

APPENDIX B: THE LINEAR STABILITY ANALYSIS

The linear stability analysis is based on the consideration of evolution of a linear perturbation $u_1=u_1(\boldsymbol{\rho},T)$ and $u_2=u_2(\boldsymbol{\rho},T)$ of the stationary state $\mathbf{(}U_1(\rho),U_2(\rho)\mathbf{)}$. The evolution equations for the perturbation are derived by linearization of the original system [system (6)] about the stationary solution. One looks for eigenfrequencies ω of the resulting linear system by setting $u_j=e^{-i\omega t}[X_j(\boldsymbol{\rho})+iY_j(\boldsymbol{\rho})]$, $j=1,2$. The appearance of an imaginary eigenfrequency means instability. In particular, by writing the perturbed solution as

$$\psi_j = e^{-i\mu_j T}[U_j(\rho)+u_j(\boldsymbol{\rho},T)], \quad j=1,2, \tag{B1}$$

using this in the system (6), and keeping only the linear terms in u_1 and u_2 we arrive at the following eigenvalue problem (consult also Refs. [33,34]):

$$\Lambda_0\begin{pmatrix}Y_1\\Y_2\end{pmatrix} = -i\omega\begin{pmatrix}X_1\\X_2\end{pmatrix}, \quad \Lambda_1\begin{pmatrix}X_1\\X_2\end{pmatrix} = i\omega\begin{pmatrix}Y_1\\Y_2\end{pmatrix},$$

$$\Lambda_n = \begin{pmatrix}L_{n1} & 0\\0 & L_{n2}\end{pmatrix}. \tag{B2}$$

Here $(j=1,2)$,

$$L_{0j} = -\mu_j - \nabla_\perp^2 + \sum_{m=1,2} g_{jm}U_m^2(\rho) + \lambda_j^2\rho^2,$$

$$L_{1j} = -\mu_j - \nabla_\perp^2 + \sum_{m=1,2} g_{jm}U_m^2(\rho) + 2g_{jj}U_j^2(\rho) + \lambda_j^2\rho^2. \tag{B3}$$

Expansion of the eigenvalue problem (B2) in the Fourier series with respect to the polar angle θ leads to an infinite series of one-dimensional eigenvalue problems of similar form for the orbital projections of the vectors $(X_1,X_2)^T$ and $(Y_1,Y_2)^T$,

$$X_j = \sum_{l\geqslant 0} X_{jl}(\rho)e^{il\theta} + \text{c.c.}, \quad Y_j = \sum_{l\geqslant 0} Y_{jl}(\rho)e^{il\theta} + \text{c.c.}, \quad j=1,2, \tag{B4}$$

with the orbital operators defined by $\Lambda_{0l}=\Lambda_0(\nabla_\perp^2\to\nabla_\rho^2 - l^2/\rho^2)$ and $\Lambda_{1l}=\Lambda_1(\nabla_\perp^2\to\nabla_\rho^2-l^2/\rho^2)$, where $\nabla_\rho^2\equiv\partial_\rho^2+\rho^{-1}\partial_\rho$. However, only a few of these 1D eigenvalue problems need to be considered to decide on the stability of the axial ground state. Indeed, first, as follows from the general criterion for the stability of the ground state in a system of nonlinear Schrödinger equations [34], in the two-component system the axial ground state is unstable if there are at least three negative eigenvalues of the operator Λ_1. For instance, if each of the first three orbital operators Λ_{1l}, $l=0,1,2$, has a negative eigenvalue, then the ground state is unstable. Second, as the orbital operators satisfy the obvious inequality $\Lambda_{1l_2} \geqslant \Lambda_{1l_1}$ (understood as the inequality for the mean values) for $l_2\geqslant l_1$, it is sufficient to consider just three orbital problems arising from Eqs. (B2) with orbital numbers $l=0,1,2$. This is the approach we adopted.

Finally, we would like to mention that the linear stability is closely related to the energy minimization (consult also Refs. [33,34]). Indeed, the operator Λ_0 is non-negative [it has two zero modes due to the phase invariance of the system (6)]. Thus, from an energetic point of view, a negative eigenvalue of the operator Λ_1 corresponds to a negative direction in the free energy functional, defined here as the Lagrange-modified energy functional $\mathcal{F}\equiv\mathcal{E}-\mu_1N_1-\mu_2N_2$, evaluated at the axially symmetric state $\mathbf{(}U_1(\rho),U_2(\rho)\mathbf{)}$, since the operator Λ_1 enters the second-order term in the free energy expansion with respect to the perturbation $\hat{u}_j=X_j(\boldsymbol{\rho})+iY_j(\boldsymbol{\rho})$, $j=1,2$:

$$\delta^2\mathcal{F} = 2\int d^2\boldsymbol{\rho}\left\{(Y_1,Y_2)\Lambda_0\begin{pmatrix}Y_1\\Y_2\end{pmatrix} + (X_1,X_2)\Lambda_1\begin{pmatrix}X_1\\X_2\end{pmatrix}\right\}. \tag{B5}$$

Taking into account that there are two independent constraints on the numbers of atoms in the two species we conclude that only two negative directions may be eliminated by the energy dependence on the numbers of atoms. Therefore, for fixed numbers of atoms, the axially symmetric state is definitely not an energy minimum if there are three (or more) negative eigenvalues of the operator Λ_1. This explains the physical origin of the above-mentioned sufficient condition for instability. We note also that the dipole-mode instability (i.e., existence of the unstable orbital mode with the orbital number $l=1$) simply means the appearance of an asymmetric state which minimizes the energy—i.e., the symmetry-breaking transition.

[1] C. J. Myatt, E. A. Burt, R. W. Ghrist, E. A. Cornell, and C. E. Wieman, Phys. Rev. Lett. **78**, 586 (1997).
[2] D. S. Hall, M. R. Matthews, J. R. Ensher, C. E. Wieman, and E. A. Cornell, Phys. Rev. Lett. **81**, 1539 (1998).
[3] J. Stenger, S. Inouye, D. M. Stamper-Kurn, H.-J. Miesner, A. Chikkatur, and W. Ketterly, Nature (London) **396**, 345 (1998).
[4] H.-J. Miesner, D. M. Stamper-Kurn, J. Stenger, S. Inouye, A. P. Chikkatur, and W. Ketterle, Phys. Rev. Lett. **82**, 2228 (1999).
[5] P. Maddaloni, M. Modugno, C. Fort, F. Minardi, and M. Inguscio, Phys. Rev. Lett. **85**, 2413 (2000).
[6] A. G. Truscott, K. E. Strecker, W. I. McAlexander, G. B. Partridge, and R. G. Hulet, Science **291**, 2570 (2001).
[7] F. Schreck, L. Khaykovich, K. L. Corwin, G. Ferrari, T. Bourdel, J. Cubizolles, and C. Salomon, Phys. Rev. Lett. **87**, 080403 (2001).
[8] G. Modugno, M. Modugno, F. Riboli, G. Roati, and M. Inguscio, Phys. Rev. Lett. **89**, 190404 (2002).
[9] G. Roati, F. Riboli, G. Modugno, and M. Inguscio, Phys. Rev. Lett. **89**, 150403 (2002).
[10] J. Goldwin, S. B. Papp, B. DeMarco, and D. S. Jin, Phys. Rev. A **65**, 021402(R) (2002).
[11] Z. Hadzibabic, C. A. Stan, K. Dieckmann, S. Gupta, M. W. Zwierlein, A. Görlitz, and W. Ketterle, Phys. Rev. Lett. **88**, 160401 (2002).
[12] J. P. Burke, Jr., J. L. Bohn, B. D. Esry, and Chris H. Greene, Phys. Rev. Lett. **80**, 2097 (1998).
[13] I. Bloch, M. Greiner, O. Mandel, Th. W. Hänsch, and T. Esslinger, Phys. Rev. A **64**, 021402 (2001).
[14] S. L. Cornish, N. R. Claussen, J. L. Roberts, E. A. Cornell, and C. E. Wieman, Phys. Rev. Lett. **85**, 1795 (2000).
[15] P. Ao and S. T. Chui, Phys. Rev. A **58**, 4836 (1998).
[16] P. Öhberg and S. Stenholm, Phys. Rev. A **57**, 1272 (1998).
[17] D. Gordon and C. M. Savage, Phys. Rev. A **58**, 1440 (1998).
[18] B. D. Esry and C. H. Greene, Phys. Rev. A **59**, 1457 (1999).
[19] J. G. Kim and E. K. Lee, Phys. Rev. E **65**, 066201 (2002).
[20] A. A. Svidzinsky and S. T. Chui, Phys. Rev. A **67**, 053608 (2003).
[21] H. Pu and N. P. Bigelow, Phys. Rev. Lett. **80**, 1134 (1998).
[22] Th. Busch, J. I. Cirac, V. M. Pérez-García, and P. Zoller, Phys. Rev. A **56**, 2978 (1997).
[23] S. K. Adhikari, Phys. Rev. A **63**, 043611 (2001); J. Phys. B **34**, 4231 (2001).
[24] K. Mølmer, Phys. Rev. Lett. **80**, 1804 (1998).
[25] N. Nygaard and K. Mølmer, Phys. Rev. A **59**, 2974 (1999).
[26] R. Roth and H. Feldmeier, Phys. Rev. A **64**, 043603 (2001).
[27] Z. Akdeniz, A. Minguzzi, P. Vignolo, and M. P. Tosi, Phys. Rev. A **66**, 013620 (2002).
[28] R. Roth and H. Feldmeier, Phys. Rev. A **65**, 021603(R) (2002).
[29] R. Roth, Phys. Rev. A **66**, 013614 (2002).
[30] L. P. Pitaevskii and S. Stringari, *Bose-Einstein Condensates in Gases* (Cambridge University Press, Cambridge, England, 2003).
[31] G. Fibich and G. Papanicolaou, SIAM (Soc. Ind. Appl. Math.) J. Appl. Math. **60**, 183 (1999).
[32] A. Gammal, T. Frederico, and L. Tomio, Phys. Rev. A **64**, 055602 (2001); A. Gammal, L. Tomio, and T. Frederico, *ibid.* **66**, 043619 (2002).
[33] E. A. Kuznetsov, A. M. Rubenchik, and V. E. Zakharov, Phys. Rep. **142**, 103 (1986).
[34] D. E. Pelinovsky and Yu. S. Kivshar, Phys. Rev. E **62**, 8668 (2000).